

Characterization of the stochastic signal originating from compact binary populations as measured by LISA

Nikolaos Karneios,^{1,2} Stanislav Babak,^{1,3} Mauro Pieroni⁴, Neil Cornish,⁵ and Tyson Littenberg⁶

¹APC, AstroParticule et Cosmologie, CNRS, Université de Paris, F-75013 Paris, France

²Department of Physics, Aristotle University of Thessaloniki, Thessaloniki 54124, Greece

³Moscow Institute of Physics and Technology, Dolgoprudny, Moscow region, Russia

⁴Blackett Laboratory, Imperial College London, SW7 2AZ, United Kingdom

⁵eXtreme Gravity Institute, Department of Physics, Montana State University,

Bozeman, Montana 59717, USA

⁶NASA Marshall Space Flight Center, Huntsville, Alabama 35812, USA



(Received 22 April 2021; accepted 29 July 2021; published 20 August 2021)

The Laser Interferometer Space Antenna (LISA) mission, scheduled for launch in the early 2030s, is a gravitational wave observatory in space designed to detect sources emitting in the millihertz band. In contrast to the present ground-based detectors, the LISA data are expected to be a signal dominated, with strong and weak gravitational wave signals overlapping in time and in frequency. Astrophysical population models predict a sufficient number of signals in the LISA band to blend together and form an irresolvable foreground noise. In this work, we present a generic method for characterizing the foreground signals originating from a given astrophysical population of coalescing compact binaries. Assuming idealized detector conditions and a perfect data analysis technique capable of identifying and removing the bright sources, we apply an iterative procedure which allows us to predict the different levels of foreground noise.

DOI: 10.1103/PhysRevD.104.043019

I. INTRODUCTION

The Laser Interferometer Space Antenna (LISA) is a space-based gravitational wave (GW) observatory mission scheduled for launch in the early 2030s [1]. Unlike currently observed GW signals, LISA sources are expected to be long-lived, with thousands of strong GW signals present in the data overlapping in time and/or in frequency. This implies that all GW signals from various sources will be have to be fit for and characterized simultaneously. The sources generating overlapping signals include supermassive black hole binaries (SMBHBs) [2,3], stellar-mass black hole binaries (SBBHs) [4–9], ultracompact binaries originating in our Galaxy (CGBs) [10–13], extreme mass ratio inspirals (EMRIs) [14–17], and a stochastic GW background that may originate from cosmological sources [18,19]. The number and density of GW sources in the LISA band present a data analysis challenge of producing a *global fit* [20], simultaneously detecting and classifying overlapping signals, which is often referred to as the “source confusion problem.”

Astrophysical population models predict a sufficiently large number of sources to form a resolution-limited GW foreground signal that could be measured by LISA even after all resolvable sources have been fit and removed from the data. The unresolved component is usually referred to as “confusion noise,” following initial studies that employed a resolvability criterion based on source density,

demanding that the number of data points equal or exceed the number of parameters required to fit each source [21,22]. Later studies showed that a reduction in signal-to-noise ratio due to the “self-noise” from other sources in the population generally has a greater impact on detectability [23], but the terms “confusion noise” and “foreground confusion” had already taken root, and we will continue to use them here.

Given the expected LISA sensitivity [24], we expect the GW confusion signal from millions of CGBs to dominate over instrumental noise between ~ 0.4 and ~ 3 mHz. These CGBs mostly comprise detached and interacting white dwarfs [13,25]. A small number of them (~ 30) have been already observed electromagnetically, and parameters of those binaries suggest that they should emit GWs in the LISA band. A subset of them should be easily detectable, and those binaries are referred to as *verification binaries*: guaranteed LISA sources which can be used to monitor performance of the instruments [26]. Models for the full population of CGBs suggests upwards of ~ 60 million binaries [27–29] in the LISA band, with only a small fraction (~ 10 thousand) of them being individually resolvable. Thus, most of those binaries will contribute to the confusion foreground signal.

Another guaranteed population of binaries in the local Universe consists of SBBHs. Merging SBBHs are observed by the LIGO and Virgo detectors, with over 40 such

systems having been reported after partial analysis of data from the third observational run [30]. Those binaries at the early stage of their inspiral emit a GW signal at the high-frequency end of LISA measurement band. While it was suggested that it might be challenging to recover such sources with LISA [31], the ensemble of these sources could potentially be another source of a confusion foreground for LISA. So far, upper bounds on the stochastic signals have been estimated by a direct extrapolation from the LIGO-Virgo event rate [5–7,32,33].

At very low frequencies, we expect a stochastic GW signal from a population of SMBHBs in sufficiently wide orbits to be emitting almost monochromatic GW signals. The SMBHB background is the one of the primary sources targeted pulsar timing arrays, which use radio emission from the ultrastable millisecond pulsars to detect GWs in the nanohertz band. The upper limits on the GW amplitude are reported in Refs. [34–37], and recent results [38] suggest the presence of a common red-noise process among the observed pulsars which might be confirmed as a GW signal in the near future. The merger of SMBHBs will be observed by LISA, and detection of a stochastic GW signal by a pulsar timing array might constrain the expected event rate of those sources in the LISA band.

The presence of astrophysical foregrounds poses a data analysis challenge for the LISA mission. Naturally, the combination of the different foreground and background signals will complicate the source separation procedures for LISA. In addition, the exact level of the confusion noise will affect the achievable precision of source parameter estimation for resolvable signals. Thus, it is of great importance to study, understand, and predict the overall shape and amplitudes of the potential foreground components of the LISA data. This will allow us to make more realistic predictions for the resolvable sources with LISA, as well as to gain a better understanding on the data analysis requirements for the mission. On the other hand, the separation and characterization of the different contributions to the foreground signal may provide additional insight into the channels of formation and evolution of astrophysical populations that generate those signals. For example, current astrophysical uncertainties for some sources translate to several orders of magnitude uncertainty in the event rate; to wit, predicted event rates for EMRIs are between a few to a few thousands per year [39], making the presence or absence of an EMRI-induced foreground an informative constraint on the underlying theory.

In this work, we present a generic method for predicting and characterization the foreground signals as measured by LISA. We begin with a combination of ideas from previous works [23,40–42], upon which we expand in two directions. First, we use updated estimates of the instrument capabilities, based on the state-of-the-art studies of the LISA design [24], and we simulate and analyze the data directly on the LISA time-delay interferometry (TDI)

[43,44] data streams. We have used both simple analytic models for the instrument noise power spectral density (PSD) and time series simulated using LISA Code [45]. Second, as described in Sec. II, we have developed a framework to perform our analysis for different types of foregrounds, generated by different types of binary sources. Then, in Secs. III and IV, we apply this methodology, as an illustrative example, to the foreground confusion signal generated by the CGBs and SBBHs, respectively. As a further demonstration, given a model to characterize the residual foreground signal, we perform a Markov Chain Monte Carlo (MCMC) analysis to infer parameters of the foreground signal which encodes information about the underlying population. We also demonstrate that resolving the bright CGB and SBBH sources leads to the separability of their respective foreground signals despite the GWs being emitted by the underlying populations overlapping in frequency between ~ 2 and ~ 5 mHz. Finally, in Sec. V, we study how the presence of two astrophysical foreground components affects the parameter estimation of resolvable signals using a Fisher information matrix approach.

II. METHODOLOGY

The methodology we followed is based on the rather strong assumption that bright sources with a signal-to-noise ratio (SNR) larger than a given threshold are detected and characterized without systematic bias or source confusion (see Ref. [20] for more refined estimates that take into account imperfect signal removal). The detection threshold is adjusted for the different source types, taking into account search and parameter estimation studies, as, for example, in Ref. [46] for CGBs and Ref. [31] for SBBHs. Assuming ideal noise conditions, where the spectral properties of the readout and test mass are identical in each link, we define the total SNR estimate for a given source as

$$\rho_{\text{tot}}^2 = \sum_K (h_K | h_K), \quad (1)$$

with $K \in \{A, E\}$ the noise-orthogonal TDI variables [43,44] and $(\cdot | \cdot)$ the noise weighted inner product expressed for two time series a and b as

$$(a|b) = 2 \int_0^\infty df [\tilde{a}^*(f) \tilde{b}(f) + \tilde{a}(f) \tilde{b}^*(f)] / \tilde{S}_n(f), \quad (2)$$

where the tilde represents the data in the Fourier frequency domain and the asterisk stands for the complex conjugate. The $\tilde{S}_n(f)$ is one-sided PSD of the noise for the different TDI variables $S_K(f)$.

One can estimate the residual confusion noise from a population of GW sources by subtracting the sources whose SNR exceeds a given detection threshold. The problem arises when one has to compute Eq. (1), where $\tilde{S}_n(f) \equiv \tilde{S}_{\text{instr}}(f) + \tilde{S}_{\text{conf}}(f)$ includes the confusion

residual GW signal $\tilde{S}_{\text{conf}}(f)$ and the instrumental noise $\tilde{S}_{\text{instr}}(f)$. A solution is to follow a methodology similar to Ref. [23] and set up an iterative process to estimate $\tilde{S}_n(f)$. The basic steps of the analysis are summarized as follows.

- (a) First, the data generation takes place either in the frequency or in the time domain, based on a predefined observation time and a given sampling frequency. We simulate the GW signals from the population of N sources drawn from a given astrophysical population model. During this process, we also the SNR of each source with respect to the adopted instrumental noise model; we refer to it as the optimal SNR of the source in isolation, ρ_i^{iso} . We will use ρ_i^{iso} as a measure of GW strength in the next step.
- (b) We estimate the confusion noise $S_{n,k}$ using either a running mean or median on the power spectrum of the data. The index k refers to the iteration number. On top of the smoothed PSD, one can also fit a polynomial model or perform spline interpolation smoothing (which we usually do). Then, assuming the SNR threshold ρ_0 , we calculate the SNR ρ_i for each source $i \in N$ using the smoothed $S_{n,k} = \tilde{S}_{\text{instr}}(f) + \tilde{S}_{\text{conf},k}(f)$ as the total noise PSD in Eq. (2). If $\rho_i > \rho_0$, the source is subtracted from the data. In this step, we make use of the previously calculated ρ_i^{iso} to accelerate the procedure: If $\rho_i^{\text{opt}} < \chi\rho_0$, we skip computation of the SNR for this (i th) source, instead automatically adding it to the confusion. Here, $\chi \leq 1$ is some safety factor. Note that we assume perfect source

identification and subtraction, which will not be achievable in practice [20].

- (c) After subtracting the brightest sources in the previous step, we return back to step (a) where we evaluate the smoothed PSD of the residuals $S_{n,k+1}$ and iterate steps (a) and (b). The algorithm stops when either no sources exceed the threshold ρ_0 or $S_{n,k+1} \simeq S_{n,k}$ based on a fractional tolerance limit, which we choose to be around $\sim 5\%$ for all frequencies and all channels. In principle, both criteria can be met at the same time. We usually choose to work with the fractional tolerance, because it accelerates convergence, since the number of sources subtracted at the final iterations of the algorithm is small.
- (d) The process converges within 5–10 iterations, resulting in the smooth estimation of the PSD for the confusion noise S_{final} . We use it to evaluate the final SNR for all subtracted source during the iterative procedure. In addition, we evaluate a projected accuracy in measuring parameters of those sources based on the Fisher information matrix (FIM). This iterative scheme is illustrated in Fig. 1(a) for the population of CGBs (see the next section for details).
- (e) Finally, we perform an MCMC analysis to fit a parameterized model for the confusion noise S_{final} to the residual.

We find that the choice of the window length for the noise estimation or the method for the final step of smoothing the residual (using either polynomial or spline fits) does not have a significant impact on the result. On the other hand,

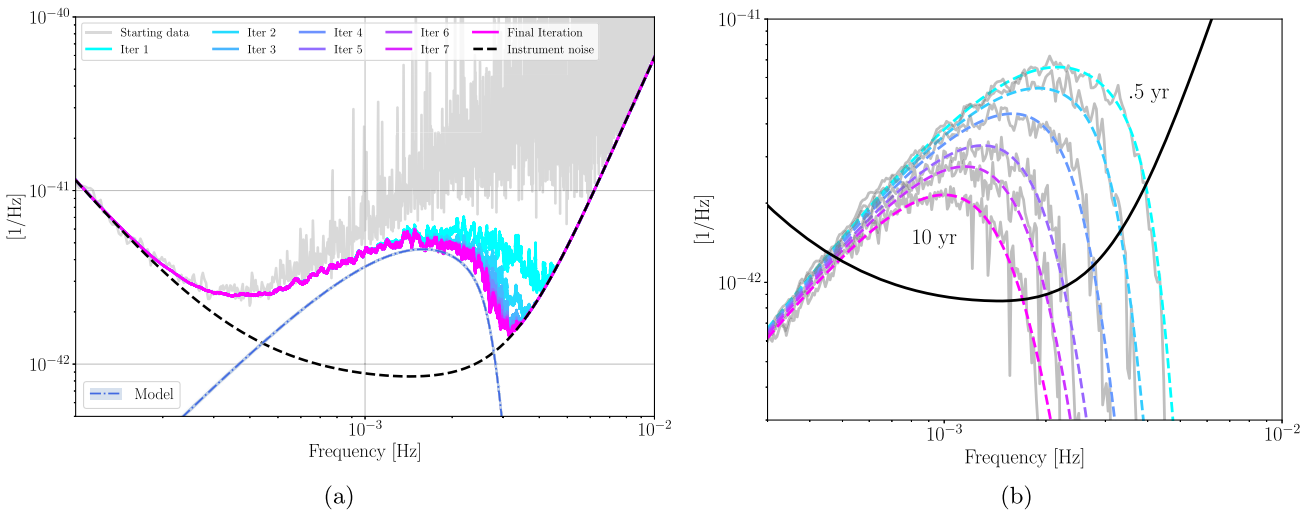


FIG. 1. (a) Illustration of the progress of the procedure for estimating the confusion noise. For the population of the CGBs described in Sec. III, it takes 6–10 iterations for the algorithm to converge, depending on the convergence tolerance criterion. The starting data are represented with the gray curve (300 segment averaged spectrum), while the final combined instrument and confusion noise is represented here in bright magenta. The dark blue dashed line represents the analytic model fit of the confusion noise component, together with the associated error bars. In this example, the observation time is $T_{\text{obs}} = 2$ yr. (b) Using the analytical model of Eq. (7) and the parameter values from Table II, we can make a prediction of the level of the confusion noise due to CGBs, depending on a given observation time. Here, we depict the power spectrum of the residual data with gray, while the colored dashed lines represent the model prediction for the given T_{obs} .

we find noticeable differences between using a running mean or median for the case of the PSD smoothing method. The PSD quantity is χ^2 distributed (i.e., has a fatter tail toward higher values), so, in principle, we should expect even in the absence of signals the smoothing method following a running mean to be larger than the running median case. We, nevertheless, perform analysis using both methods and report below our findings.

To conclude this section, we comment on the working assumption employed in the definition of the procedure. We have assumed idealized conditions for the instrumental noise: The noise is stationarity, and there are no gaps, glitches, or instrumental “lines” (monochromatic or almost monochromatic signal of instrumental or environmental origin). All these artifacts either could be identified and removed [47–50] and/or will affect the SNR threshold for a reliable detection. Note that we do not need to assume that the instrumental noise is known, as we estimate it at each step of iteration, and the confusion GW signal is just yet another noise component (from the SNR computation point of view). We also could deal directly with Michelson X , Y , Z TDI data streams, evaluate the cross spectra, and either diagonalize the noise matrix (producing new A , E , T TDI) or work directly with the nondiagonal noise matrix.

Of greater consequence is our assumption of idealized data analysis that can exactly identify the GW signals above a certain threshold. There is an ongoing effort within the LISA data challenge (LDC) project to demonstrate and evaluate the performance of various data analysis techniques. Current results look very encouraging [46,51–53], and we are confident that we will be able to reliably detect GW sources in the LISA data, but, nevertheless, the procedure here represents an unattainable ideal. Our analysis neglects the effect of the instrument and confusion noise on the source identification itself: The best recovered parameters from the model will be different from the true values due to the presence of noise [20]. Furthermore, the observed catalog will unavoidably have some contamination due to several sources being fit with a single model waveform, especially early on during the LISA observing campaign [46]. As a result, removing the estimated GW sources will inevitably remove a small portion of the noise with it and/or leave behind some residual signal [20]. An idea to make our simulation more realistic while still computationally tractable would be to build a small Markov chain, forming posteriors for the source (or collection of overlapped sources). Another solution would be to estimate the covariance matrix of the parameters based on a FIM calculation and then draw the given “solution” for each source from a multivariate Gaussian distribution. We relegate these more elaborate approaches to future work and consider the results presented here as a zero-order approximation which is fast to run and gives a good starting point for a more detailed analysis.

Last but not least, we want to comment on the simulated data. We have to choose the GW model to simulate the LISA data. Naturally, one would be tempted to use a simplified and fast waveform model to compute the GW signal; however, the final result might strongly depend on the simulated LISA data. For example, use of higher-order modes in the simulated signal could significantly affect the conclusion, even if those modes are not strong for each individual source. The same concerns the simulation of numerous subthreshold events: In simulating the data, we need to include also very weak sources; in other words, the catalog should be *complete* and extend to include sources which merge beyond the simulated span of the data.

III. APPLICATION TO THE CASE OF COMPACT GALACTIC BINARIES

In this section, we apply our methodology to the population of the CGBs. We study the properties of the confusion signal, after subtracting the “loud” counterparts, as a function of observation time T_{obs} . We assume that the orbital period evolves slowly and, thus, can use a very simple model for the GW signal where the phase is decomposed in a Taylor series. The signal in the source frame can be presented as

$$h_+^s = \mathcal{A}(1 + \cos^2 i) \cos(\Phi(t)), \quad (3)$$

$$h_x^s = 2\mathcal{A} \cos i \sin(\Phi(t)), \quad (4)$$

with

$$\Phi(t) = \phi_0 + 2\pi f_0 t + \pi \dot{f}_0 t. \quad (5)$$

Here, ϕ_0 is the initial GW phase, and we neglect all but the first frequency derivative \dot{f}_0 , as it is sufficient for evaluation of the foreground signal. Higher-order derivatives are seldom detectable for the assumed CGB population [54]. \mathcal{A} is the GW strain amplitude and i the inclination. The signal describes early inspiral evolution; however, due to mass transfer in the interacting binaries, the system could also “outspiral” (negative frequency derivative). We have assumed that the binaries are in circular orbits, which is expected for the vast majority of systems. We have also neglected the presence of exoplanets or (in general) a third perturbing body [55,56]. In principle, provided that a model that would include the effects of the third body on the waveform is available [57], it would be straightforward to include those systems in our study. An addition like this does not affect our main objective: evaluating the number of resolvable systems and characterizing the residual confusion foreground.

Next, we need to transform the waveform to the Solar System barycenter, by assuming the latitude β and longitude λ ecliptic coordinates of the source, and introducing the polarization angle ψ . We follow exactly the polarization

and angle conventions of Ref. [58] and an implementation based on Ref. [59].

We chose to work with the catalogs of the Radler LISA data challenge dataset [58,60]. This catalog contains the signal of 29857650 CGBs, generated by the population models of Refs. [61,62].

For a given set of T_{obs} and SNR threshold ρ_0 , we generate idealized datasets directly in the frequency domain. The data are simplified in the sense that they do not contain any other type of GW signals. In addition to the signals, we simulated instrumental noise using the LISA Code simulator [45]. The PSD of the noise could either be empirically determined from the simulated data or we assume the analytic fit [58]. We have run the iterations described in Sec. II for $\rho_0 = \{5, 7\}$, and $T_{\text{obs}} = \{0.5, 1, 2, 4, 6, 10\}$ yr. At the end of each run, we have the set of the subtracted sources and smoothed CGB foreground signal.

A. Recovered compact galactic binary sources

As expected, the number of recovered sources greatly depends on the chosen SNR threshold ρ_0 and the LISA observation time T_{obs} . For the given LISA configuration [24] and setting $\rho_0 = \{5, 7\}$, we recover the number of sources displayed in Table I. The numbers are reported for two methods of evaluating the smoothed PSD: running median and running mean.

B. Confusion noise due to compact galactic binaries

We use an empirical analytical model for the estimated confusion foreground given as

$$S_{\text{gal}} = \frac{A}{2} f^{-7/3} e^{-(f/f_1)^\alpha} (1 + \tanh((f_{\text{knee}} - f)/f_2)). \quad (6)$$

The first two terms $\propto Af^{-7/3}$ are the expected spectral shape generated from a population binaries evolving due to GW emission [41], the second factor accounts for the loss of stochasticity as we move to higher frequencies, and the factor in the brackets (with hyperbolic tangent) reflects that after (roughly) $f \geq f_{\text{knee}}$ we should be able to resolve and

TABLE I. The recovered number of sources as a function of the LISA observation time T_{obs} for two methods of smoothing PSD.

T_{obs} [yr]	No. of sources recovered			
	Running mean		Running median	
	$\rho_0 = 5$	$\rho_0 = 7$	$\rho_0 = 5$	$\rho_0 = 7$
0.5	8031	4491	8850	5111
1	14170	8487	14918	9305
2	22681	14206	23849	15441
4	35891	22951	37684	25025
6	45925	30097	48179	32702

subtract all GBs. The fit for each observation time T_{obs} is shown in Fig. 1(b).

The six fitting parameters for the confusion noise model are two scaling frequencies f_1 and f_2 , the knee frequency f_{knee} , the amplitude A , and a “smoothness” parameter α . The overall amplitude A is a property of the population of GBs. The frequency f_2 and α are expected to be a property of a population *and* the SNR threshold we use. The two remaining parameters f_1 and f_{knee} are expected to also have a strong dependence on the observation time: Indeed, the longer we observe, the more CGBs become resolvable and, therefore, could be subtracted.

We have simulated LISA TDI time series data for a total observation duration of $T_{\text{obs,max}} = 10$ yr and then estimated the confusion noise for different fractions of $T_{\text{obs,max}}$. We have found that the f_1 and f_{knee} parameters of Eq. (6) can be well approximated as the following functions of observation duration T_{obs} :

$$\begin{aligned} \log_{10}(f_1) &= a_1 \log_{10}(T_{\text{obs}}) + b_1 \quad \text{and} \\ \log_{10}(f_{\text{knee}}) &= a_k \log_{10}(T_{\text{obs}}) + b_k, \end{aligned} \quad (7)$$

with a_1 , a_k , b_1 , and b_k being amplitude calibration parameters. For this part of the analysis, since our aim is to report on the point estimates for such a model, we have used simple optimization algorithms [63,64] to find the maximum of a joint χ^2 function that combines the datasets of different durations. Their values are reported in Table II. This empirical analytic fit works rather well for observation durations above 1 yr and improves with the observational duration. The minimum observation time we have checked was 3 months. Note that the GW signals from the population of CGBs are cyclostationary, meaning that the signal is modulated during the annual orbital motion of LISA: with its antenna pattern function pointing toward or away from the Galactic Center, where the majority of the sources are found. This nonstationarity is reflected in deviations from the analytic fit, which depends on where

TABLE II. The parameters of the empirical model describing the confusion noise due to the unresolved CGBs signal. We report on both methods of performing the data smoothing: running mean and median.

Parameter	Estimated			
	Running mean		Running median	
	$\rho_0 = 5$	$\rho_0 = 7$	$\rho_0 = 5$	$\rho_0 = 7$
a_1	-0.16	-0.25	-0.15	-0.15
a_k	-0.34	-0.27	-0.34	-0.37
b_1	-2.78	-2.70	-2.78	-2.72
b_k	-2.53	-2.47	-2.55	-2.49
$A \times 10^{-44}$	1.15	1.14	1.14	1.15
f_2	0.00059	0.00031	0.00059	0.00067
α	1.66	1.80	1.66	1.56

we terminate the observations during the first year. Nonetheless, as seen in Fig. 1(b), the fit is still quite satisfactory.

C. Fit of the Galactic model to the confusion noise

As a proof of principle, we have also looked at the inverse problem. We have assumed that the numerically evaluated CGB foreground is the result of LISA observations (reduced by removing the bright sources). Next, we evaluate the residual signal and infer parameters of the simple Galactic model given by Eq. (6) using Bayesian sampling techniques. For this purpose, we perform a preprocessing procedure similar to the one employed in Refs. [65–67].

Given the full data stream, we first convert the data to Ω_{GW} units using

$$h^2 \Omega_{\text{GW}} \equiv \frac{4\pi^2 f^3}{3(H_0/h)^2} S(f), \quad (8)$$

H_0 being the Hubble parameter as observed today and h its dimensionless normalization. We then cut it into N_c data segments having the same duration of around 11.5 d corresponding to 10^{-6} Hz and average over segments.¹ At this point, in order to further lower the computational complexity of the problem, we coarse-grain (i.e., bin) the data to a less dense set (in the following denoted f_{ij}^k and D_{ij}^k) by performing an inverse variance weighting of the data using the noise as an estimate for the variance (see Sec. III. 1 in Ref. [67] for details). In particular, for each decade in frequency above 10^{-4} Hz, we pass from the initial 10^{-6} Hz linear spacing to 250 evenly logarithmically spaced frequency points. Similarly to Ref. [67], we then define our likelihood as a combination of a Gaussian and of a log-normal distribution which accounts for skewness contributions, giving a more accurate result for the model parameters [67–71]. The data are modeled as

$$D_{ij}^{\text{th}}(f_{ij}^k) = h^2 \Omega_{\text{GW}}(f_{ij}^k, \vec{\theta}_s) + h^2 \Omega_n(f_{ij}^k, \vec{\theta}_n), \quad (9)$$

where Ω_{GW} is the model of the spectral shape of the signal component [here, Eq. (6) in Ω_{GW} units²], $\vec{\theta}_s$ is the vector of parameters for the signal, Ω_n is the instrument noise [i.e., $S_{\text{instr}}(f)$] in Ω_{GW} units, and $\vec{\theta}_n$ is the vector of parameters for the noise. In the following analysis, we fix $\vec{\theta}_n$ at their nominal values.

¹For a dataset in the frequency domain with frequency resolution $\sim 1/T_{\text{obs}}$, for a given frequency, say, f_i , this corresponds to averaging over data points with $f_i - 5 \times 10^{-7}$ Hz $\leq f \leq f_i + 5 \times 10^{-7}$ Hz.

²Notice that for this analysis, in order to work with order one numbers, rather than the parameter A appearing in Eq. (6), we constrain the $\log_{10}(h^2 \Omega_*) = \log_{10}[4\pi^2 A/3/(H_0/h)^2]$.

Finally, we sample the parameter space using Polychord [72,73] via its interface with Cobaya [74]. The Polychord sampler belongs to the family of nested sampling algorithms, where it uses slice sampling techniques in order to efficiently sample parameter spaces of high dimensionality. Our particular problem here is not very demanding in terms of posterior multimodality. We, therefore, executed the algorithm using $5 \times \dim = 40$ live points and with a tolerance criterion for convergence set to 10^{-3} (based on the evidence calculation). The results of this investigation, which are analyzed and visualized using GetDist [75], are shown in Fig. 2.

To conclude this section, we discuss the performance of the phenomenological model in Eq. (6) to fit the data. As is possible to see from Fig. 3, the best fit for this model (shown in blue) is quite accurately matching the data (gray shade) for all frequencies where the confusion residual signal from the CGBs dominates over the instrumental noise (i.e., for frequencies larger than $\sim 5 \times 10^{-4}$). On the other hand, we notice that at lower frequencies the template overestimates the level of confusion noise with respect to the result obtained from the simulated catalog. In order to look for a possible source for this deviation, we performed further parameter estimation assuming the spectral tilt [the $-7/3$ in Eq. (6)] to be another free parameter of the model. In this case, we obtained a slightly larger value for the tilt (see the pink curve in Fig. 3), which leads to a better fit to the data in the low-frequency band. We have found the value of the spectral tilt to be $n_s = 1.12 \pm 0.01$ in Ω_{GW} units. While a detailed analysis of this deviation could motivate further investigations, it lies beyond the scope of the present work, and, thus, it is left for future studies on the topic.

IV. STOCHASTIC SIGNAL DUE TO STELLAR MASS BINARY BLACK HOLES

Since the initial successes of the ground-based GW detectors, there have been studies focusing on the possibility of measuring GWs from SBBHs [76–79]. Based on the current understanding of the SBBH population, the expected number of detectable sources in the LISA band ranges from $\mathcal{O}(1)$ to $\mathcal{O}(10)$. These sources will be in the LISA band for several years before entering and merging in the band covered by ground-based interferometers [8,76,78,80]. LISA is sensitive to the early inspiral stage of orbital evolution of SBBHs, where the orbit shrinks very slowly, and, therefore, most of the binaries stay in the observing band throughout the LISA observation time.

Depending on the population model, the SBBH signals may fill the LISA observing band down to ~ 3 mHz, thus partially overlapping with the high-frequency tail of the CGB population. At these frequencies, the CGB population transitions from being a confusion-dominated population to the regime where all sources are individually identifiable [81]. The region of potential overlap between the CGB

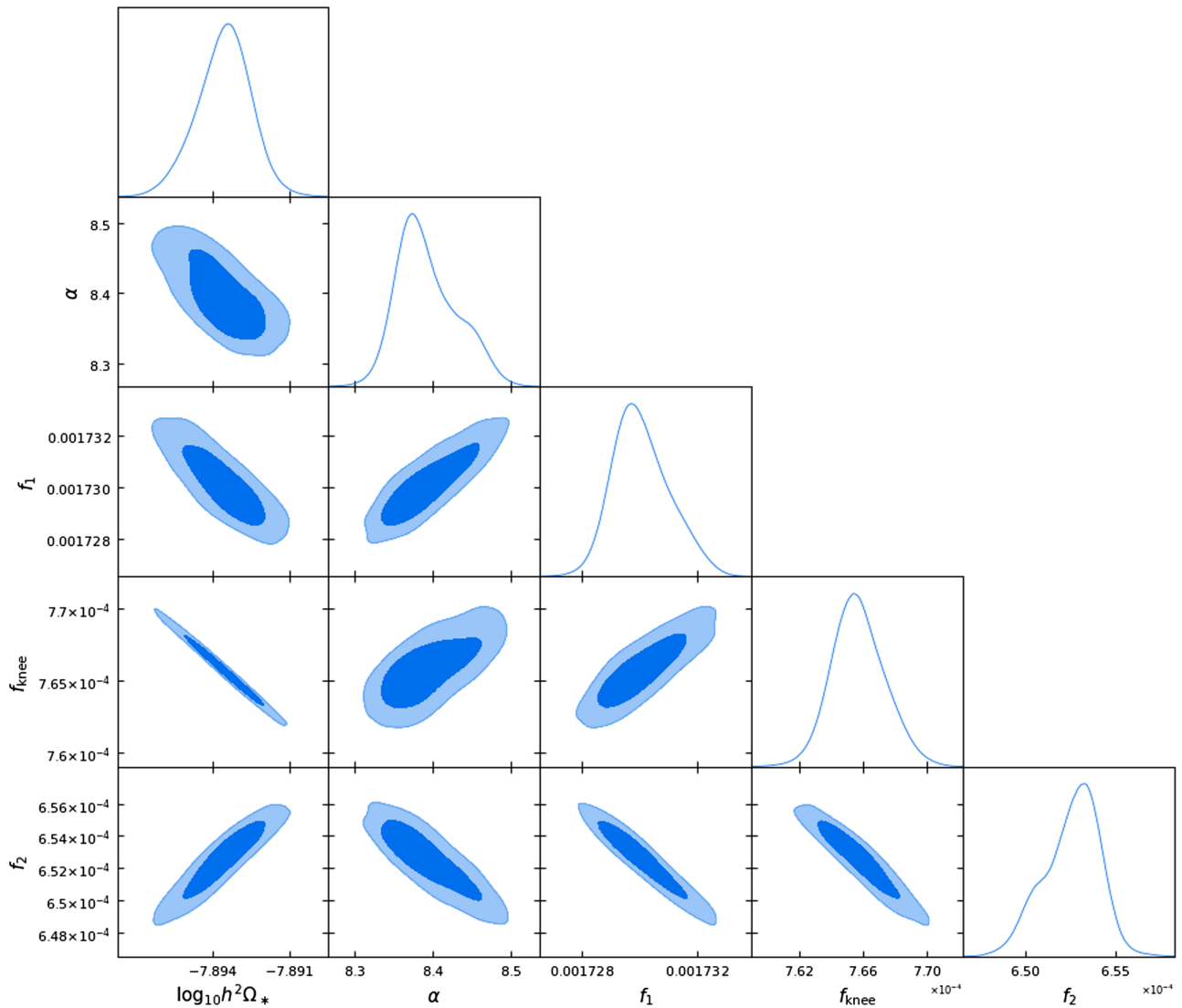


FIG. 2. The 2D projections of the posterior distributions of the parameters of model of Eq. (6), as sampled with MCMC methods (see the text for details). The fit was performed on a dataset with duration of 10 yr, after subtracting the bright sources with SNR threshold $\rho_0 = 5$.

residual and the SBBH population reduces with the LISA mission duration, as more individual CGBs sources are being resolved and subtracted.

The population of SBBHs observed by LISA depends on the merger rate of SBBHs in the local Universe, \mathcal{R} , expressed as the number of mergers per comoving volume (Gpc^3) per year. \mathcal{R} is currently best estimated from the mergers detected during LIGO-Virgo observing runs, which also provide inferences on the mass, mass ratio, and spin distribution [9]. These observations are translated into an event rate in the LISA band [8] as

$$\frac{d^2n}{d\mathcal{M}dz} = \mathcal{R} \frac{dV_c(z)}{dz} \frac{1}{1+z} p(\mathcal{M}), \quad (10)$$

where $p(\mathcal{M})$ is the probability distribution function for the chirp mass \mathcal{M} . We could include other parameters like

mass ratio, spins, etc., but for this simple example we restrict our attention only to the chirp mass. We have used the original prescription [8] to generate a catalog of SBBH sources emitting in the LISA band.

Note that we did not use the most up-to-date population estimates [30], and the mock populations used here serve illustration purposes; more elaborate analysis is underway and will be published later [82]. Instead, we have used the catalogs of SBBHs available with the first LDC dataset [58,60]. We simulate a dataset with duration of $T_{\text{obs}} \sim 2.7$ yr, using the PhenomD waveform model [83]. We have used the same idealized assumptions about the instrument noise and subtraction fidelity as for the population of CGBs and apply the same iterative procedure to the population of SBBHs.

Using a SNR threshold $\rho_0 = 15$, we do not find any detectable binaries, confirming the results of Ref. [31].

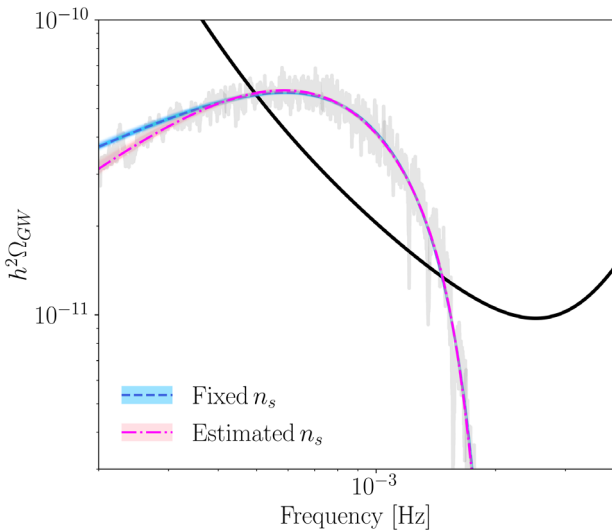


FIG. 3. Fit of the two models we considered to the confusion residuals signal from CGBs. The first model, following faithfully Eq. (6), assumes a fixed spectral index of $-7/3$ in strain units or $n_s = 2/3$ in Ω_{GW} units (shown in blue). The pink data refer to a model where the spectral index n_s is a free parameter of the fit (see the text for details).

The results for different values of ρ_0 are summarized in Fig. 4. It is likely that the threshold $\rho_0 = 15$ is an overestimate for the detection threshold, which relies on the grid-based (template bank) search which takes into account only local correlations. On the other hand, the threshold $\rho_0 = 5$ is an underestimate, assuming that the volume of parameter space with high likelihood is small [53,76]. The results of the iterative subtraction are presented in Fig. 4.

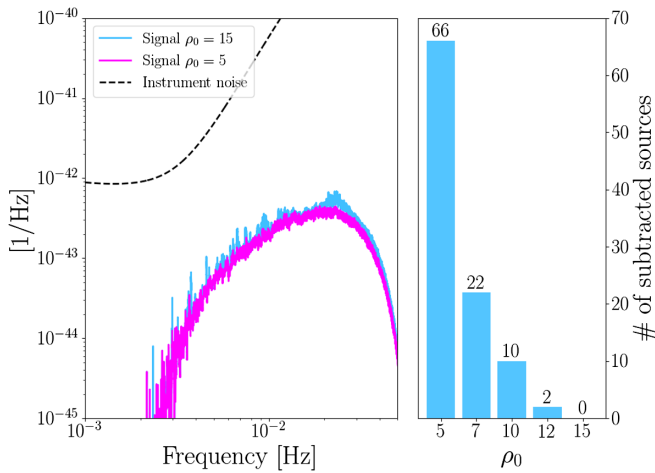


FIG. 4. Left: the residual confusion noise created by a population of SBBHs for the SNR thresholds $\rho_0 = \{5, 15\}$. Both curves have been estimated using a running median on the data. Right: the number of resolvable sources that are detected and subtracted from the data for different values of SNR threshold ρ_0 .

V. COMBINING THE POPULATIONS FROM DIFFERENT GRAVITATIONAL WAVE SOURCES

The same methodology and analysis principles that we used in the previous sections (Secs. III and IV) can be followed for characterizing a foreground signal that originates from a combination of different types of sources. In that case, at step (c) of the algorithm described in Sec. II, we iterate over all types of sources and compare the individual SNR $\rho_{i,t}$ with $\rho_{0,t}$, where the t index refers to the given source type. Thus, the measured confusion signal would be the direct result of the superposition of the foreground signals from all given types of sources. This translates to $\tilde{S}_n(f) \equiv \tilde{S}_{\text{instr}}(f) + \sum_t \tilde{S}_{\text{conf},t}(f)$, which would yield higher levels of the unresolved foreground GW signal. Naturally, we expect that this would affect the source recovery and parameter estimation for the recovered sources. Note that this procedure does not account for the possibility of misidentifying one source type for another where the populations overlap. For demonstration purposes, we choose to work with the two populations that we have been using so far: the CGBs and the SBBHs.

The two types of populations, while in both cases the majority of their individual sources are almost monochromatic, have inherently different characteristics. For the detached Galactic binaries, we took a population based on the model described in Ref. [29], while a population of interacting binaries (with mass transfer) is based on Ref. [27]. This model does not include extra-Galactic sources, but those should be a minority. The population of SBBHs is fully phenomenological and described in Ref. [8]. It assumes a simple log-uniform mass function $5\text{--}100 M_\odot$ with a merger rate $\approx 35 \text{ yr}^{-1} \text{ Gpc}^{-3}$ and uniform in comoving volume with the range of $0 < z < 2$. In Ref. [8], it is argued that this population is vague enough to include several possible channels of formation. We should emphasize that we use this model for illustrative purposes; the method works exactly the same way for any population of binaries as an input (including populations of binary massive black holes and/or extreme mass ratio inspirals). Independently of the details of populations, the confusion noise due to CGBs is expected to dominate at low frequencies $\lesssim 3 \times 10^{-3} \text{ Hz}$ and to drop at larger frequencies (because of subtraction of loud sources), while the confusion noise due to SBBHs is subdominant at low frequencies and becomes relevant at $f \gtrsim 3 \times 10^{-3} \text{ Hz}$ (see Figs. 1 and 4).

Using the two catalogs, we generated a LISA time series dataset with a duration of $T_{\text{obs}} = 2.67 \text{ yr}$, and we applied the algorithm as described in Sec. II. As already mentioned, the difference here is that at each iteration we compute the SNR of both types of sources with respect to the overall background noise. We choose an SNR threshold for each type of source, in particular, $\rho_{0,\text{cgb}} = 7$ and $\rho_{0,\text{sbbh}} = \{5, 8, 10, 12, 15\}$. The number of sources that

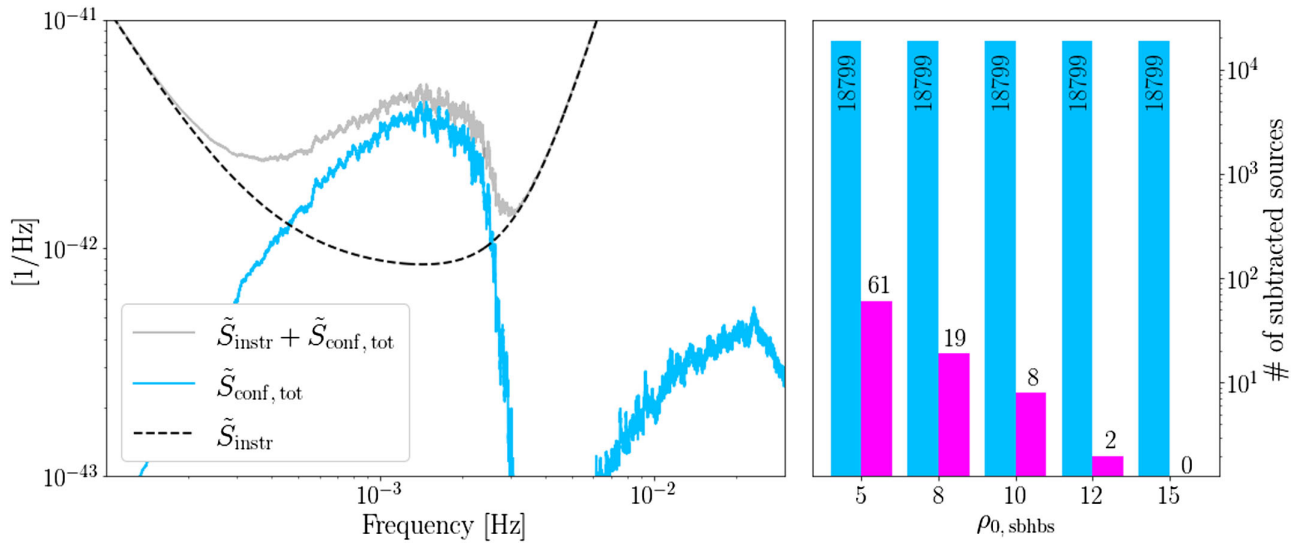


FIG. 5. Left: the total signal of the unresolved sources from both populations of CGBs and SBBHs (shown in blue), after subtracting the brightest sources. The signal plus instrumental noise is shown with gray color. Right: the number of subtracted sources for different assumptions about the SNR threshold for the SBBHs, ρ_0, sbbh (represented with the pink bars). For the given population and observation duration, it is fairly evident that for $\rho_0, \text{sbbh} > 15$ there are not SBBHs recovered from the data. The number of CGB sources that were subtracted (blue) is the same for all cases, indicating that the total SBBH residual confusion signal is not strong enough to affect their recovery. Here, we assumed $\rho_0, \text{cgb} = 7$.

were subtracted (i.e., $\rho_{i,t} > \rho_{0,t}$) for each case are presented in Fig. 5. From our previous investigation on the same population of SBBHs, we expected a similar residual confusion signal, i.e., few to no sources subtracted for high values of ρ_0 . This is still valid in this investigation as well.

Concerning the CGBs, we notice that almost the same number of sources are recovered as in Sec. III. This was also expected, due to the very low residual confusion signal of the SBBH component of the data, which does not impact significantly the overall measured confusion signal $\tilde{S}_n(f)$. But, even in this case, we would expect to measure the impact of multiple components of stochastic signals to the recovered errors of the parameters. As described in Sec. II, at the end of each run, we make use of a Fisher matrix formalism in order to get an estimate of the CGB parameters errors of the recovered sources. The comparison of the relative errors of the parameters compared to the ideal case of a single type of population is shown in Fig. 6. It is fairly evident that, indeed, the precision of the CGBs that are recovered is minimally affected by the presence of a foreground signal generated by SBBHs, as described in Ref. [8]. The reason lies in the characteristics of the two underlying populations. First, as we have already seen, the confusion signal due to the SBBH population is small relative to the instrument noise and, thus, does not significantly impact the precision with which we estimate the parameters of the CGBs. In addition, the two populations used in this study, after subtraction of the “loudest” sources, only minimally overlap to 2–3 mHz frequency regime.

VI. DISCUSSION

We have developed a methodology to perform estimates of the residual confusion signals, originating from different types of binary sources, as measured by LISA. We have expanded on the methodology presented in Ref. [23], which is based on the assumption that sources with a SNR above the detection threshold will be characterized and subtracted from the data. We have applied this methodology, as a demonstration, to datasets containing either CGBs or SBBHs. For the CGBs, we have updated the existing models that describe the confusion signal using up-to-date LISA characteristics and noise models. For the case of the SBBH signal, we have confirmed the findings of Ref. [31], which indicated that the population model of Ref. [8] would yield events with quite low SNR, making the detection, characterization, and subtraction of such sources challenging.

Furthermore, we have demonstrated that one can use the same methodology to characterize the confusion signal that is generated from different types of source populations. To do that, we have combined the components of the GW signatures of both the CGBs and the SBBHs that were used in the previous investigations. The results showed that, for the given observation duration, the resulting confusion signal had an impact on the recovered sources of the weaker component, i.e., the one originating from the SBBHs. The number of recovered CGBs was not affected. Furthermore, for this particular case we tested, the accuracy of the parameters of the recovered CGBs was also not significantly affected. This was verified by computing the errors

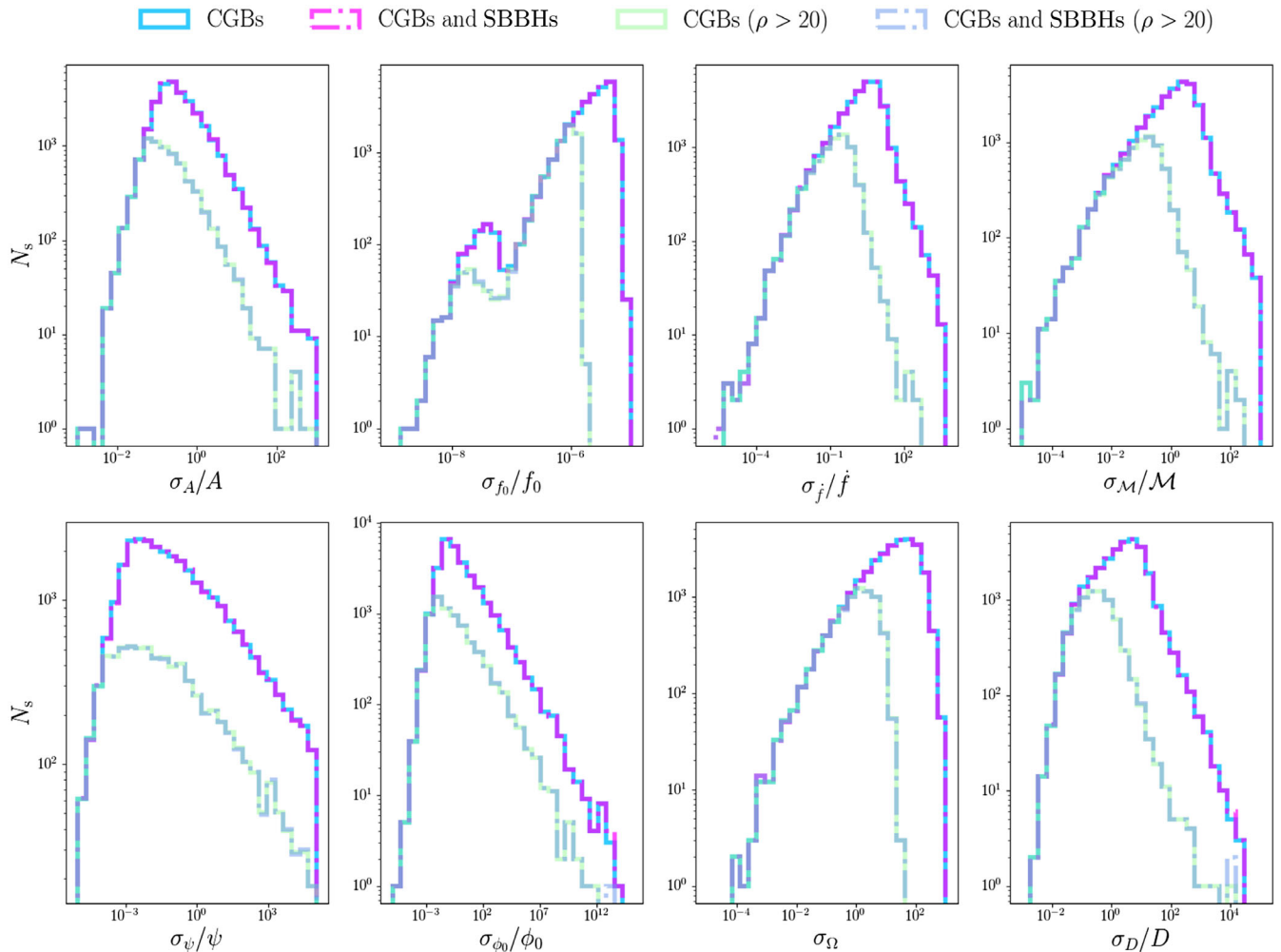


FIG. 6. Histograms of the recovered errors for the parameters of the subtracted CGBs. The optimal case, where there are only CGBs in the data, is depicted with blue, while the relative errors of the same population with the presence of SBBHs is shown in pink. The same type of histograms are plotted for the brighter ($\rho > 20$) sources in green and light blue, respectively.

of the parameters of each binary with respect to the resulting confusion noise, using a Fisher matrix approach. The methodology is efficient and computationally inexpensive, since the computational bottleneck was found to be just the template calculation.

However, one should mention that this approach begins with idealized assumptions about the instrument noise. Indeed, the noise is assumed to be Gaussian and stationary for the duration of the measurement, while the data quality is assumed optimal, i.e., uninterrupted and without any noise transients. At the same time, we have adopted a SNR criterion for defining the detection thresholds of the given sources. While this is proven to be a very useful tool for our purposes, it ignores realistic data analysis challenges, such as complications due to the overlap of multiple signals. Moreover, the source subtraction is assumed to be optimal as well, which means that the residuals are considered to be ideal. Even so, we expect the resulting characterization of confusion signal to be an optimistic case of analyses such

as Ref. [46]. Search methods, such as the ones developed in Ref. [46], are capable of searching and subtracting candidate sources by utilizing the Bayesian evidence ratio (encapsulated in the algorithm formalism), which is a statistically more appropriate method of analysis.

Finally, this work was developed with the aim of creating a tool to characterize the foreground signal, in terms of spectral shape and its evolution with the LISA mission duration, for any given potential binary population that could contribute to it. In that sense, it presents as a useful, fast, and practical tool for zeroth-order approximation of unresolvable astrophysical foreground signals measured by LISA.

ACKNOWLEDGMENTS

The authors acknowledge the work of the LDC group. For this study, both the LDC software and datasets were used. The work of M. P. was supported by Science and

Technology Facilities Council Grants No. ST/P000762/1 and No. ST/T000791/1. M. P. acknowledges support by the European Union's Horizon 2020 Research Council Grant

No. 724659 MassiveCosmo ERC-2016-COG. N. C. appreciates the support of NASA LISA foundation Science Grant No. 80NSSC19K0320.

-
- [1] P. Amaro-Seoane *et al.*, arXiv:1702.00786.
- [2] J. G. Baker, J. Centrella, D.-I. Choi, M. Koppitz, and J. van Meter, *Phys. Rev. Lett.* **96**, 111102 (2006).
- [3] E. Berti, *Classical Quantum Gravity* **23**, S785 (2006).
- [4] B. P. Abbott *et al.* (LIGO Scientific and Virgo Collaborations), *Phys. Rev. X* **9**, 031040 (2019).
- [5] B. P. Abbott *et al.* (LIGO Scientific and Virgo Collaborations), *Phys. Rev. Lett.* **118**, 121101 (2017).
- [6] A. I. Renzini and C. R. Contaldi, *Phys. Rev. Lett.* **122**, 081102 (2019).
- [7] J. Aasi *et al.* (LIGO Scientific and Virgo Collaborations), *Phys. Rev. D* **91**, 022003 (2015).
- [8] A. Sesana, *Phys. Rev. Lett.* **116**, 231102 (2016).
- [9] R. Abbott *et al.* (LIGO Scientific and Virgo Collaborations), *Astrophys. J. Lett.* **900**, L13 (2020).
- [10] W. A. Hiscock, S. L. Larson, J. R. Routzahn, and B. Kulick, *Astrophys. J.* **540**, L5 (2000).
- [11] V. Kalogera, R. Narayan, D. N. Spergel, and J. H. Taylor, *Astrophys. J.* **556**, 340 (2001).
- [12] G. Nelemans, L. Yungelson, and S. F. P. Zwart, *Astron. Astrophys.* **375**, 890 (2001).
- [13] T. R. Marsh, *Classical Quantum Gravity* **28**, 094019 (2011).
- [14] C. P. L. Berry, R. H. Cole, P. Cañizares, and J. R. Gair, *Phys. Rev. D* **94**, 124042 (2016).
- [15] Y. Wang, Y. Shang, and S. Babak, *Phys. Rev. D* **86**, 104050 (2012).
- [16] A. J. K. Chua and J. R. Gair, *Classical Quantum Gravity* **32**, 232002 (2015).
- [17] L. Barack and C. Cutler, in *Laser Interferometer Space Antenna. Proceedings of the 5th International LISA Symposium and 38th ESLAB Symposium, Noordwijk, Netherlands, 2004* (2005) [arXiv:gr-qc/0502052].
- [18] C. Caprini and D. G. Figueira, *Classical Quantum Gravity* **35**, 163001 (2018).
- [19] T. Regimbau and S. A. Hughes, *Phys. Rev. D* **79**, 062002 (2009).
- [20] T. Robson and N. Cornish, *Classical Quantum Gravity* **34**, 244002 (2017).
- [21] P. L. Bender and D. Hils, *Classical Quantum Gravity* **14**, 1439 (1997).
- [22] L. Barack and C. Cutler, *Phys. Rev. D* **70**, 122002 (2004).
- [23] S. E. Timpano, L. J. Rubbo, and N. J. Cornish, *Phys. Rev. D* **73**, 122001 (2006).
- [24] LISA Science Study Team, Technical Report No. ESA-L3-EST-SCI-RS-001, ESA, 2018.
- [25] A. Stroeer and A. Vecchio, *Classical Quantum Gravity* **23**, S809 (2006).
- [26] T. Kupfer, V. Korol, S. Shah, G. Nelemans, T. R. Marsh, G. Ramsay, P. J. Groot, D. T. H. Steeghs, and E. M. Rossi, *Mon. Not. R. Astron. Soc.* **480**, 302 (2018).
- [27] G. Nelemans, L. R. Yungelson, and S. F. P. Zwart, *Mon. Not. R. Astron. Soc.* **349**, 181 (2004).
- [28] V. Korol, O. Koop, and E. M. Rossi, *Astrophys. J.* **866**, L20 (2018).
- [29] V. Korol, E. M. Rossi, P. J. Groot, G. Nelemans, S. Toonen, and A. G. A. Brown, *Mon. Not. R. Astron. Soc.* **470**, 1894 (2017).
- [30] R. Abbott *et al.* (LIGO Scientific and Virgo Collaborations), *Phys. Rev. X* **11**, 021053 (2021).
- [31] C. J. Moore, D. Gerosa, and A. Klein, *Mon. Not. R. Astron. Soc.: Lett.* **488**, L94 (2019).
- [32] B. Abbott *et al.*, *Astrophys. J.* **659**, 918 (2007).
- [33] B. P. Abbott *et al.* (LIGO Scientific and Virgo Collaborations), *Phys. Rev. D* **93**, 042005 (2016).
- [34] Z. Arzoumanian *et al.*, *Astrophys. J.* **821**, 13 (2016).
- [35] Z. Arzoumanian *et al.*, *Astrophys. J.* **859**, 47 (2018).
- [36] J. R. Gair, J. D. Romano, and S. R. Taylor, *Phys. Rev. D* **92**, 102003 (2015).
- [37] L. Lentati *et al.*, *Mon. Not. R. Astron. Soc.* **453**, 2577 (2015).
- [38] Z. Arzoumanian *et al.* (NANOGrav Collaboration), *Astrophys. J. Lett.* **905**, L34 (2020).
- [39] S. Babak, J. Gair, A. Sesana, E. Barausse, C. F. Sopuerta, C. P. Berry, E. Berti, P. Amaro-Seoane, A. Petiteau, and A. Klein, *Phys. Rev. D* **95**, 103012 (2017).
- [40] S. Nissanke, M. Vallisneri, G. Nelemans, and T. A. Prince, *Astrophys. J.* **758**, 131 (2012).
- [41] N. Cornish and T. Robson, *J. Phys. Conf. Ser.* **840**, 012024 (2017).
- [42] J. Crowder and N. J. Cornish, *Phys. Rev. D* **75**, 043008 (2007).
- [43] M. Tinto and S. V. Dhurandhar, *Living Rev. Relativity* **8**, 4 (2005).
- [44] T. A. Prince, M. Tinto, S. L. Larson, and J. W. Armstrong, *Phys. Rev. D* **66**, 122002 (2002).
- [45] A. Petiteau, G. Auger, H. Halloin, O. Jeannin, E. Plagnol, S. Pireaux, T. Regimbau, and J.-Y. Vinet, *Phys. Rev. D* **77**, 023002 (2008).
- [46] T. B. Littenberg, N. J. Cornish, K. Lackeos, and T. Robson, *Phys. Rev. D* **101**, 123021 (2020).
- [47] C. Pankow *et al.*, *Phys. Rev. D* **98**, 084016 (2018).
- [48] T. Robson and N. J. Cornish, *Phys. Rev. D* **99**, 024019 (2019).
- [49] N. J. Cornish, T. B. Littenberg, B. Bécsy, K. Chatzioannou, J. A. Clark, S. Ghonge, and M. Millhouse, *Phys. Rev. D* **103**, 044006 (2021).
- [50] K. Chatzioannou, N. Cornish, M. Wijngaarden, and T. B. Littenberg, *Phys. Rev. D* **103**, 044013 (2021).
- [51] S. Marsat, J. G. Baker, and T. Dal Canton, *Phys. Rev. D* **103**, 083011 (2021).

- [52] N. J. Cornish and K. Shuman, *Phys. Rev. D* **101**, 124008 (2020).
- [53] A. Toubiana, S. Marsat, S. Babak, J. Baker, and T. Dal Canton, [arXiv:2007.08544](https://arxiv.org/abs/2007.08544).
- [54] T. B. Littenberg and N. Yunes, *Classical Quantum Gravity* **36**, 095017 (2019).
- [55] T. Robson, N. J. Cornish, N. Tamanini, and S. Toonen, *Phys. Rev. D* **98**, 064012 (2018).
- [56] C. Danielski, V. Korol, N. Tamanini, and E. Rossi, *Astron. Astrophys.* **632**, A113 (2019).
- [57] S. Naoz, *Annu. Rev. Astron. Astrophys.* **54**, 441 (2016).
- [58] S. Babak and A. Petiteau, APC Paris Technical Report No. LISA-LCST-SGS-MAN-002, 2020, <https://lisa-ldc.lal.in2p3.fr/static/data/pdf/LDC-manual-002.pdf>.
- [59] N. J. Cornish and T. B. Littenberg, *Phys. Rev. D* **76**, 083006 (2007).
- [60] LISA data challenges, the Radler dataset, <https://lisa-ldc.lal.in2p3.fr/ldc>, accessed: 2019-04-09.
- [61] V. Korol *et al.*, *Astron. Astrophys.* **638**, A153 (2020).
- [62] G. Nelemans, *ASP Conf. Ser.* **467**, 27 (2013), [arXiv:1302.0138](https://arxiv.org/abs/1302.0138).
- [63] J. A. Nelder and R. Mead, *Comput. J.* **7**, 308 (1965).
- [64] P. Virtanen, R. Gommers, T. E. Oliphant, M. Haberland, T. Reddy, D. Cournapeau, E. Burovski, P. Peterson, W. Weckesser, J. Bright *et al.*, *Nat. Methods* **17**, 261 (2020).
- [65] C. Caprini, D. G. Figueroa, R. Flauger, G. Nardini, M. Peloso, M. Pieroni, A. Ricciardone, and G. Tasinato, *J. Cosmol. Astropart. Phys.* **11** (2019) 017.
- [66] M. Pieroni and E. Barausse, *J. Cosmol. Astropart. Phys.* **07** (2020) 021; **09** (2020) E01.
- [67] R. Flauger, N. Karnesis, G. Nardini, M. Pieroni, A. Ricciardone, and J. Torrado, *J. Cosmol. Astropart. Phys.* **01** (2021) 059.
- [68] J. Bond, A. H. Jaffe, and L. Knox, *Astrophys. J.* **533**, 19 (2000).
- [69] J. Sievers *et al.*, *Astrophys. J.* **591**, 599 (2003).
- [70] L. Verde *et al.* (WMAP Collaboration), *Astrophys. J. Suppl. Ser.* **148**, 195 (2003).
- [71] S. Hamimeche and A. Lewis, *Phys. Rev. D* **77**, 103013 (2008).
- [72] W. Handley, M. Hobson, and A. Lasenby, *Mon. Not. R. Astron. Soc.* **450**, L61 (2015).
- [73] W. Handley, M. Hobson, and A. Lasenby, *Mon. Not. R. Astron. Soc.* **453**, 4385 (2015).
- [74] J. Torrado and A. Lewis, *J. Cosmol. Astropart. Phys.* **05** (2021) 057.
- [75] A. Lewis, [arXiv:1910.13970](https://arxiv.org/abs/1910.13970).
- [76] A. Toubiana *et al.*, *Phys. Rev. Lett.* **126**, 101105 (2021).
- [77] K. Jani, D. Shoemaker, and C. Cutler, *Nat. Astron.* **4**, 260 (2020).
- [78] A. Toubiana, S. Marsat, S. Babak, J. Baker, and T. Dal Canton, *Phys. Rev. D* **102**, 124037 (2020).
- [79] S. Banerjee, *Phys. Rev. D* **102**, 103002 (2020).
- [80] P. Dayal, E. M. Rossi, B. Shiralilou, O. Piana, T. R. Choudhury, and M. Volonteri, *Mon. Not. R. Astron. Soc.* **486**, 2336 (2019).
- [81] A. Lamberts, S. Blunt, T. B. Littenberg, S. Garrison-Kimmel, T. Kupfer, and R. E. Sanderson, *Mon. Not. R. Astron. Soc.* **490**, 5888 (2019).
- [82] P. Marcoccia *et al.*, The stochastic signal of stellar origin black hole binaries as measured by LISA (to be published).
- [83] S. Khan, S. Husa, M. Hannam, F. Ohme, M. Pürrer, X. J. Forteza, and A. Bohé, *Phys. Rev. D* **93**, 044007 (2016).